

Stabilizing soliton-based multichannel transmission with frequency dependent linear gain-loss

Debananda Chakraborty¹, Avner Peleg², and Quan M. Nguyen³

¹*Department of Mathematics, New Jersey City University,
Jersey City, New Jersey, 07305, USA*

²*Department of Basic Sciences, Afeka College of Engineering, Tel Aviv, 69988, Israel and*

³*Department of Mathematics, International University,
Vietnam National University-HCMC, Ho Chi Minh City, Vietnam*

Abstract

We report several major theoretical steps towards realizing stable long-distance multichannel soliton transmission in Kerr nonlinear waveguide loops. We find that transmission destabilization in a single waveguide is caused by resonant formation of radiative sidebands and investigate the possibility to increase transmission stability by optimization with respect to the Kerr nonlinearity coefficient γ . Moreover, we develop a general method for transmission stabilization, based on frequency dependent linear gain-loss in Kerr nonlinear waveguide couplers, and implement it in two-channel and three-channel transmission. We show that the introduction of frequency dependent loss leads to significant enhancement of transmission stability even for non-optimal γ values via decay of radiative sidebands, which takes place as a dynamic phase transition. For waveguide couplers with frequency dependent linear gain-loss, we observe stable oscillations of soliton amplitudes due to decay and regeneration of the radiative sidebands.

PACS numbers: 42.65.Tg, 42.81.Dp, 42.81.Qb

I. INTRODUCTION

The rates of transmission of information in broadband optical waveguide systems can be significantly increased by transmitting many pulse sequences through the same waveguide [1–3]. This is achieved by the wavelength-division-multiplexing (WDM) method, where each pulse sequence is characterized by the central frequency of its pulses, and is therefore called a frequency channel. Applications of these WDM or multichannel systems include fiber optics communication lines [1–3], data transfer between computer processors through silicon waveguides [4, 5], and multiwavelength lasers [6, 7]. Since pulses from different frequency channels propagate with different group velocities, interchannel pulse collisions are very frequent, and can therefore lead to severe transmission degradation [1]. Soliton-based transmission is considered to be advantageous compared with other transmission formats, due to the stability and shape-preserving properties of the solitons, and as a result, has been the focus of many studies [1–3]. These studies have shown that effects of Kerr nonlinearity on interchannel collisions, such as cross-phase modulation and four-wave-mixing, are among the main impairments in soliton-based WDM fiber optics transmission. Furthermore, various methods for mitigation of Kerr-induced effects, such as filtering and dispersion-management, have been developed [2, 3]. However, the problem of achieving stable long-distance propagation of optical solitons in multichannel Kerr nonlinear waveguide loops remains unresolved. The challenge in this case stems from two factors. First, any radiation emitted by the solitons stays in the waveguide loop, and therefore, the radiation accumulates. Second, the radiation emitted by solitons from a given channel at frequencies of the solitons in the other channels undergoes unstable growth and develops into radiative sidebands. Due to radiation accumulation and to the fact that the sidebands form at the frequencies of the propagating solitons it is very difficult to suppress the instability. In the current paper, we report several major steps towards a solution of this important problem.

In Refs. [8–13], we studied soliton propagation in Kerr nonlinear waveguide loops in the presence of dissipative perturbations due to delayed Raman response and nonlinear gain-loss. We showed that transmission stabilization can be realized at short-to-intermediate distances, but that at large distances, the transmission becomes unstable, and the soliton sequences are destroyed. Additionally, in Ref. [10], we noted that destabilization is caused by resonant formation of radiative sidebands due to cross-phase modulation. However, the central

problems of quantifying the dependence of transmission stability on physical parameter values and of developing general methods for transmission stabilization against Kerr-induced effects were not addressed. In the current paper we take on these problems for two-channel and three-channel transmission by performing extensive simulations with a system of coupled nonlinear Schrödinger (NLS) equations. We first study transmission in a single lossless waveguide and investigate the possibility to increase transmission stability by optimization with respect to the value of the Kerr nonlinearity coefficient. We then demonstrate that significant enhancement of transmission stability can be achieved in waveguide couplers with frequency dependent linear loss and gain and analyze the stabilizing mechanisms. This stabilization is realized without dispersion-management or filtering.

II. THE COUPLED-NLS PROPAGATION MODEL

We consider propagation of N sequences of optical pulses in an optical waveguide in the presence of second-order dispersion, Kerr nonlinearity, and frequency dependent linear gain-loss. We assume a WDM setup, where the pulses in each sequence propagate with the same group velocity and frequency, but where the group velocity and frequency are different for pulses from different sequences. The propagation is then described by the following system of N coupled-NLS equations [1, 10]:

$$i\partial_z\psi_j + \partial_t^2\psi_j + \gamma|\psi_j|^2\psi_j + 2\gamma\sum_{k\neq j}|\psi_k|^2\psi_j = i\mathcal{F}^{-1}(g_j(\omega)\hat{\psi}_j)/2, \quad (1)$$

where ψ_j is the envelope of the electric field of the j th sequence, $1 \leq j \leq N$, z is propagation distance, t is time, ω is frequency, γ is the Kerr nonlinearity coefficient, and the sum over k extends from 1 to N [14]. In Eq. (1), $g_j(\omega)$ is the linear gain-loss experienced by the j th sequence, $\hat{\psi}_j$ is the Fourier transform of ψ_j with respect to time, and \mathcal{F}^{-1} is the inverse Fourier transform. The second term on the left-hand side of Eq. (1) is due to second-order dispersion, the third term describes self-phase modulation and intrasequence cross-phase modulation, while the fourth term describes intersequence cross-phase modulation. The term on the right-hand side of Eq. (1) is due to linear gain-loss. The optical pulses in the j th sequence are fundamental solitons of the unperturbed NLS equation $i\partial_z\psi_j + \partial_t^2\psi_j + \gamma|\psi_j|^2\psi_j = 0$. The envelopes of these solitons are given by $\psi_{sj}(t, z) = \eta_j \exp(i\chi_j) \text{sech}(x_j)$, where $x_j = (\gamma/2)^{1/2}\eta_j(t - y_j - 2\beta_j z)$, $\chi_j = \alpha_j + \beta_j(t - y_j) + (\gamma\eta_j^2/2 - \beta_j^2)z$, and η_j, β_j, y_j ,

and α_j are the soliton amplitude, frequency, position, and phase.

Notice that Eq. (1) describes both propagation in a single waveguide and propagation in a waveguide coupler, consisting of N close waveguides [15]. In waveguide coupler transmission, each waveguide is characterized by its linear gain-loss function $g_j(\omega)$. The form of $g_j(\omega)$ is chosen such that radiation emission effects are mitigated, while the soliton patterns remain intact. In particular, we choose the form

$$g_j(\omega) = -g_L + \frac{1}{2} (g_{eq} + g_L) [\tanh \{\rho [\omega - \beta_j(0) + W/2]\} - \tanh \{\rho [\omega - \beta_j(0) - W/2]\}], \quad (2)$$

where $1 \leq j \leq N$, and $\beta_j(0)$ is the initial frequency of the j th sequence solitons. The constants g_L , g_{eq} , ρ , and W satisfy $g_L > 0$, $g_{eq} \geq 0$, $\rho \gg 1$, and $\Delta\beta > W > 1$, where $\Delta\beta$ is the intersequence frequency difference. We note that the condition $\Delta\beta > 1$ is typical for soliton-based WDM transmission experiments [16–20]. Figure 1 shows typical linear gain-loss functions $g_1(\omega)$ and $g_2(\omega)$ for a two-channel waveguide coupler with $g_L = 0.5$, $g_{eq} = 3.9 \times 10^{-4}$, $\beta_1(0) = -5$, $\beta_2(0) = 5$, $W = 5$ and $\rho = 10$ (these parameters are used in the numerical simulations, whose results are shown in Fig. 8). In the limit as $\rho \gg 1$, $g_j(\omega)$ can be approximated by a step function, which is equal to g_{eq} inside a frequency interval of width W centered about $\beta_j(0)$, and to $-g_L$ elsewhere:

$$g_j(\omega) \simeq \begin{cases} g_{eq} & \text{if } \beta_j(0) - W/2 < \omega \leq \beta_j(0) + W/2, \\ g_L & \text{elsewhere.} \end{cases} \quad (3)$$

The approximate expression (3) helps clarifying the advantages of using the linear gain-loss function (2) for transmission stabilization. Indeed, the relatively strong linear loss g_L leads to efficient suppression of radiative sideband generation outside of the frequency interval $(\beta_j(0) - W/2, \beta_j(0) + W/2]$. Furthermore, the relatively weak linear gain g_{eq} in the frequency interval $(\beta_j(0) - W/2, \beta_j(0) + W/2]$ compensates for the strong loss outside of this interval and in this manner enables soliton propagation without amplitude decay. In practice, we first determine the values of g_L , W , and ρ by performing simulations with Eqs. (1) and (2) with $g_{eq} = 0$, while looking for the set that yields the longest stable propagation distance. Once g_L , W , and ρ are found, we determine g_{eq} by requiring $\eta_j(z) = \eta_j(0) = \text{const}$ for $1 \leq j \leq N$ throughout the propagation. More specifically, we use the adiabatic perturbation theory for the NLS soliton (see, e.g., Ref. [3]) to derive the following equation for the rate of change

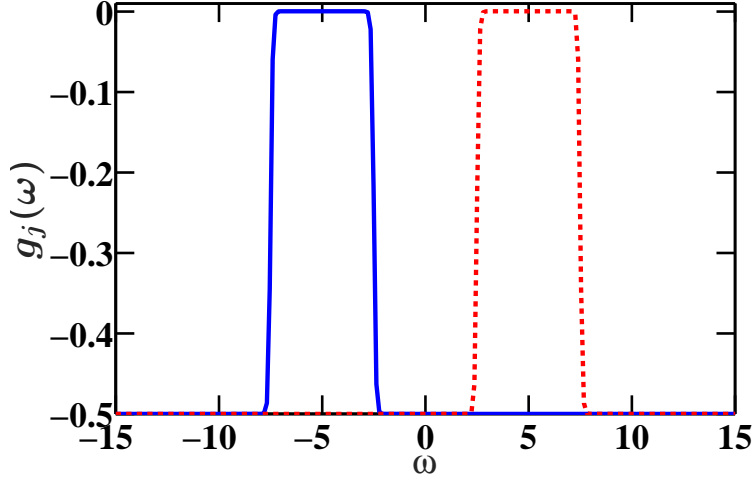


FIG. 1: An example for the frequency dependent linear gain-loss functions $g_j(\omega)$ defined by Eq. (2) in a two-channel waveguide coupler. The solid blue and dashed red lines correspond to $g_1(\omega)$ and $g_2(\omega)$, respectively.

of η_j with z due to the linear gain-loss (2):

$$\frac{d\eta_j}{dz} = \left[-g_L + (g_{eq} + g_L) \tanh \left(\frac{\pi W}{(8\gamma)^{1/2} \eta_j} \right) \right] \eta_j. \quad (4)$$

Requiring $\eta_j(z) = \eta_j(0) = \text{const}$, we obtain the following expression for g_{eq} :

$$g_{eq} = \left\{ \left[\tanh \left(\frac{\pi W}{(8\gamma)^{1/2} \eta_j(0)} \right) \right]^{-1} - 1 \right\} g_L. \quad (5)$$

Since different pulse sequences propagate with different group velocities, the solitons undergo a large number of intersequence collisions. Due to the finite length of the waveguide and the finite separation between adjacent solitons in each sequence, the collisions are not completely elastic. Instead, the collisions lead to emission of continuous radiation with peak power that is inversely proportional to the intersequence frequency difference $\Delta\beta$. The emission of continuous radiation in multiple collisions eventually leads to pulse pattern distortion and to transmission destabilization. In the current paper, we analyze the dependence of transmission stability on physical parameter values and develop waveguide setups, which lead to significant enhancement of transmission stability.

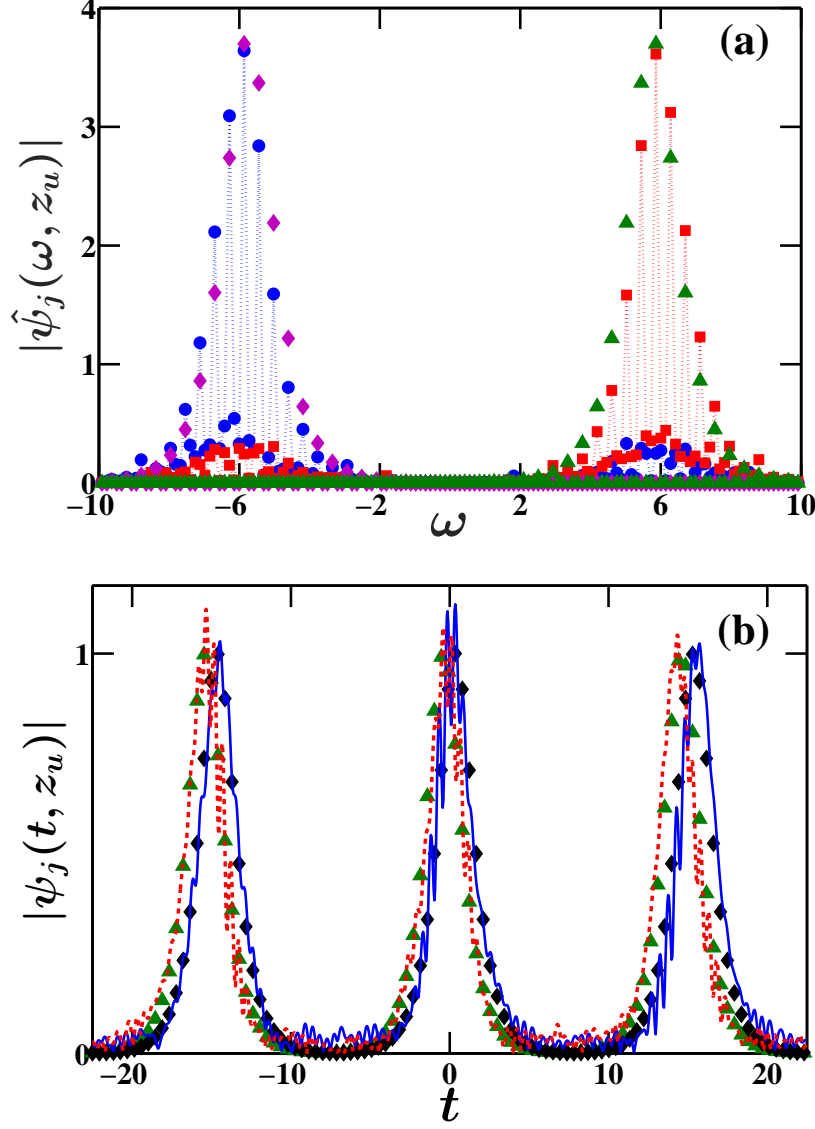


FIG. 2: (a) The Fourier transforms of the soliton patterns at the onset of instability $|\hat{\psi}_j(\omega, z_u)|$, where $z_u = 470$, for two-channel transmission in a single lossless waveguide with $\gamma = 2$, $T = 15$, and $\Delta\beta = 12$. The blue circles and red squares represent $|\hat{\psi}_j(\omega, z_u)|$ with $j = 1, 2$, obtained by numerical solution of Eq. (1), while the magenta diamonds and green triangles correspond to the theoretical prediction. (b) The soliton patterns at the onset of instability $|\psi_j(t, z_u)|$ for two-channel transmission with the parameters used in (a). The solid blue and dashed red lines correspond to $|\psi_j(t, z_u)|$ with $j = 1, 2$, obtained by the simulations, while the black diamonds and green triangles correspond to the theoretical prediction.

III. NUMERICAL SIMULATIONS

A. Introduction

To investigate transmission stability, we numerically integrate the system (1), using the split-step method with periodic boundary conditions [1]. The use of periodic boundary conditions means that the simulations describe pulse dynamics in a closed waveguide loop. The initial condition is in the form of N periodic sequences of $2K+1$ solitons with amplitudes $\eta_j(0)$, frequencies $\beta_j(0)$, and zero phases:

$$\psi_j(t, 0) = \sum_{k=-K}^K \frac{\eta_j(0) \exp[i\beta_j(0)(t - kT)]}{\cosh[(\gamma/2)^{1/2}\eta_j(0)(t - kT)]}, \quad (6)$$

where $1 \leq j \leq N$, T is the time-slot width, and $N = 2$ or $N = 3$. This initial condition represents the typical situation in multichannel soliton-based transmission [1–3]. To maximize the stable propagation distance, we choose $\beta_1(0) = -\beta_2(0)$ for a two-channel system, and $\beta_1(0) = -\beta_3(0)$ and $\beta_2(0) = 0$ for a three-channel system. This choice is based on extensive numerical simulations with Eq. (1) with the right-hand-side set equal to zero and different values of $\beta_j(0)$. For concreteness, we present here the results of numerical simulations with parameter values $T = 15$, $\eta_j(0) = 1$, $K = 1$, and a final transmission distance $z_f = 5000$. We emphasize, however, that similar results are obtained with other values of the physical parameters. That is, the results reported in this section are not very sensitive to the values of K , $\eta_j(0)$, and T , as long as $\eta_j(0)$ is not much smaller than or much larger than 1, and as long as $T > 10$.

B. Two-channel transmission

We start by considering two-channel transmission in a single lossless waveguide. Simulations with Eq. (1) with $N = 2$ show stable propagation at short-to-intermediate distances and transmission destabilization at long distances. As seen in Fig. 2, the instability first appears as fast temporal oscillations in the soliton patterns, which is caused by resonant formation of radiative sidebands with frequencies $\beta_2(0)$ for $j = 1$ and $\beta_1(0)$ for $j = 2$. The growth of the radiative sidebands with increasing z eventually leads to the destruction of the soliton patterns. We note that when each soliton sequence propagates through the waveguide on its own, no radiative sidebands develop and no instability is observed up to distances

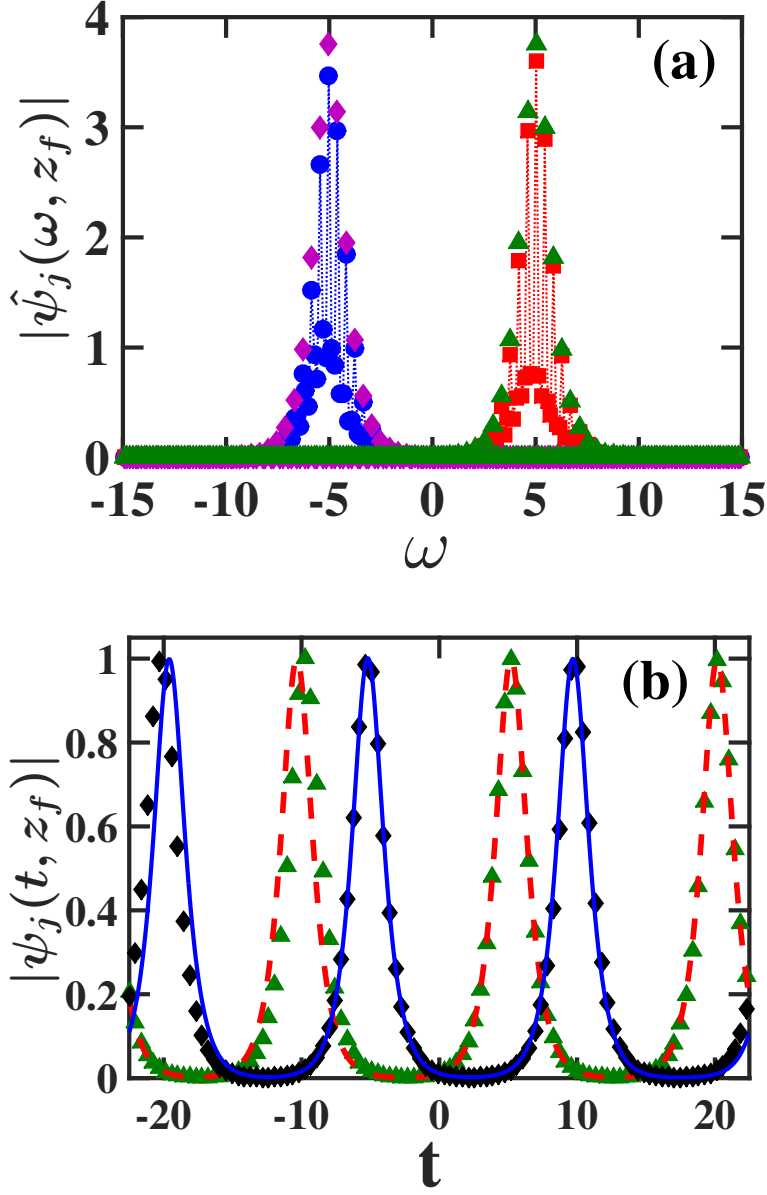


FIG. 3: (a) The Fourier transforms of the soliton patterns at the final propagation distance $|\hat{\psi}_j(\omega, z_f)|$, where $z_f = 20000$, in the case where each soliton sequence propagates on its own through a lossless waveguide. The values of the physical parameters are $\beta_1(0) = -5$, $\beta_2(0) = 5$, $\gamma = 2$, and $T = 15$. The symbols are the same as in Fig. 2(a). (b) The soliton patterns at the final propagation distance $|\psi_j(t, z_f)|$ for the single-sequence propagation setup considered in (a). The symbols are the same as in Fig. 2(b).

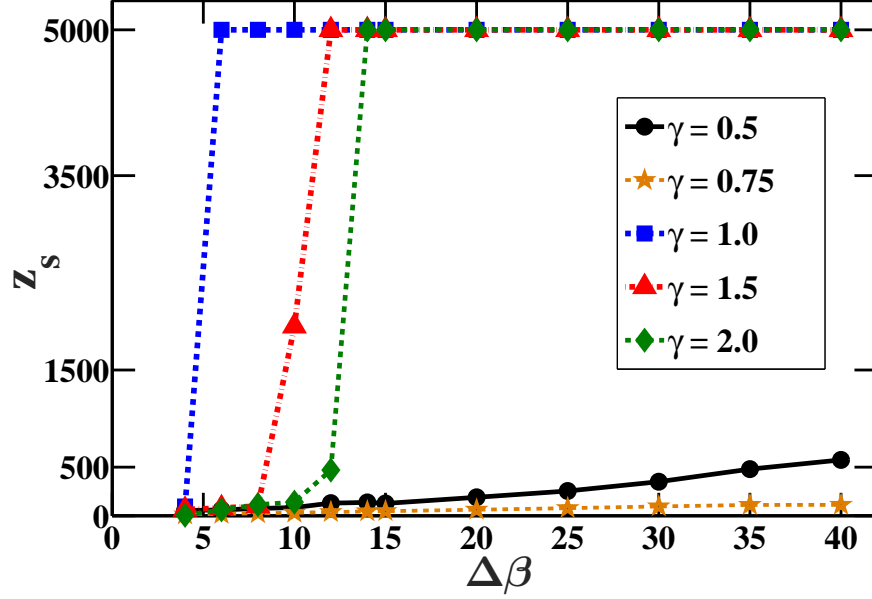


FIG. 4: Stable propagation distance z_s vs frequency spacing $\Delta\beta$ for two-channel transmission in a single lossless waveguide with $T = 15$. The black circles, orange stars, blue squares, red triangles, and green diamonds represent the results obtained by the simulations for $\gamma = 0.5, 0.75, 1.0, 1.5$, and 2.0 , respectively.

as large as $z = 20000$ (see Fig. 3). Thus, the instability is caused by the Kerr-induced interaction in interchannel collisions, i.e., it is associated with the intersequence cross-phase modulation terms $2\gamma|\psi_k|^2\psi_j$ in Eq. (1).

An important question about the transmission concerns the dependence of transmission stability on the value of the Kerr nonlinearity coefficient. In particular, we would like to find if there is an optimal value of γ , which leads to minimization of radiative sideband generation and to maximization of transmission stability. To answer this question, we define the stable propagation distance z_s as the distance z_u at which instability develops, if $z_u < z_f$, and as z_f , if no instability is observed throughout the propagation. That is, $z_s = z_u$, if $z_u < z_f$ (instability is observed), and $z_s = z_f$, if $z_u \geq z_f$ (instability is not observed). We then carry out simulations with Eq. (1) for $N = 2$, $0.5 \leq \gamma \leq 2$, and $4 \leq \Delta\beta \leq 40$, and plot z_s vs frequency spacing $\Delta\beta$. The results of the simulations are shown in Fig. 4. It is seen that z_s increases with increasing $\Delta\beta$, in accordance with the decrease of intersequence cross-phase modulation effects with increasing frequency spacing [16]. Moreover, for all frequency differences $\Delta\beta$ in the interval $4 \leq \Delta\beta \leq 40$, the z_s values obtained with $\gamma = 1$ are larger

than or equal to the z_s values achieved with $\gamma \neq 1$. Thus, $\gamma = 1$ is the optimal value of the Kerr nonlinearity coefficient. Based on these results and results of simulations with other sets of physical parameters, we conclude that for two-channel systems, there indeed exists an optimal value of the Kerr nonlinearity coefficient, which minimizes radiative sideband generation and yields the longest stable propagation distance.

Since the radiative sideband for the j th sequence forms at frequency $\beta_k(0)$ of the other sequence, it is very difficult to suppress radiative instability in a single waveguide by frequency dependent gain-loss. The situation is very different in waveguide coupler transmission, since in this case one can employ a different gain-loss profile for each waveguide, with strong loss for all frequencies outside of a frequency interval centered about $\beta_j(0)$. We therefore turn to consider waveguide couplers with frequency dependent linear loss, and show that in this case, significant enhancement of transmission stability can be achieved, even for non-optimal γ values. For this purpose, we numerically solve Eqs. (1) and (2) with $N = 2$ and $g_{eq} = 0$ for different γ values and $4 \leq \Delta\beta \leq 15$. Here we present the results obtained for $\gamma = 2$, $T = 15$, $g_L = 0.5$, $\rho = 10$, and $W = \Delta\beta/2$. Similar results are obtained with other choices of the physical parameter values. Figure 5(a) shows the stable propagation distance z_s vs frequency spacing $\Delta\beta$ as obtained in the simulations for two-channel waveguide coupler transmission along with the value obtained for transmission in a single lossless waveguide. We note that for $\Delta\beta \geq 8$, $z_s = z_f = 5000$, i.e., the transmission is stable throughout the propagation. Moreover, the z_s values obtained for waveguide coupler transmission are larger than the values obtained for single waveguide transmission by factors ranging between 172.2 for $\Delta\beta = 4$ and 2.22 for $\Delta\beta = 13$. Additionally, as seen in Fig. 5(b), the solitons retain their shape throughout the propagation.

We now turn to analyze the z dependence of soliton amplitudes for propagation in the waveguide coupler, since this analysis provides insight into the processes involved in transmission stabilization. We find three remarkably different dependences of soliton amplitudes on z in the frequency spacing intervals $4 \leq \Delta\beta < 8$, $8 \leq \Delta\beta < 14$, and $\Delta\beta \geq 14$. Figure 6(a) shows the $\eta_j(z)$ curves obtained by the simulations for three representative cases, $\Delta\beta = 4$, $\Delta\beta = 12$, and $\Delta\beta = 14$. For $\Delta\beta = 4$ and $\Delta\beta = 14$, the soliton amplitudes decrease gradually to their final values. In contrast, for $\Delta\beta = 12$, soliton amplitudes gradually decrease for $0 \leq z < 150$, but then undergo a steep decrease in the interval $150 \leq z \leq 175$, followed by another gradual decrease for $175 < z \leq 5000$ [see Figures 6(a) and 6(b)]. To explain

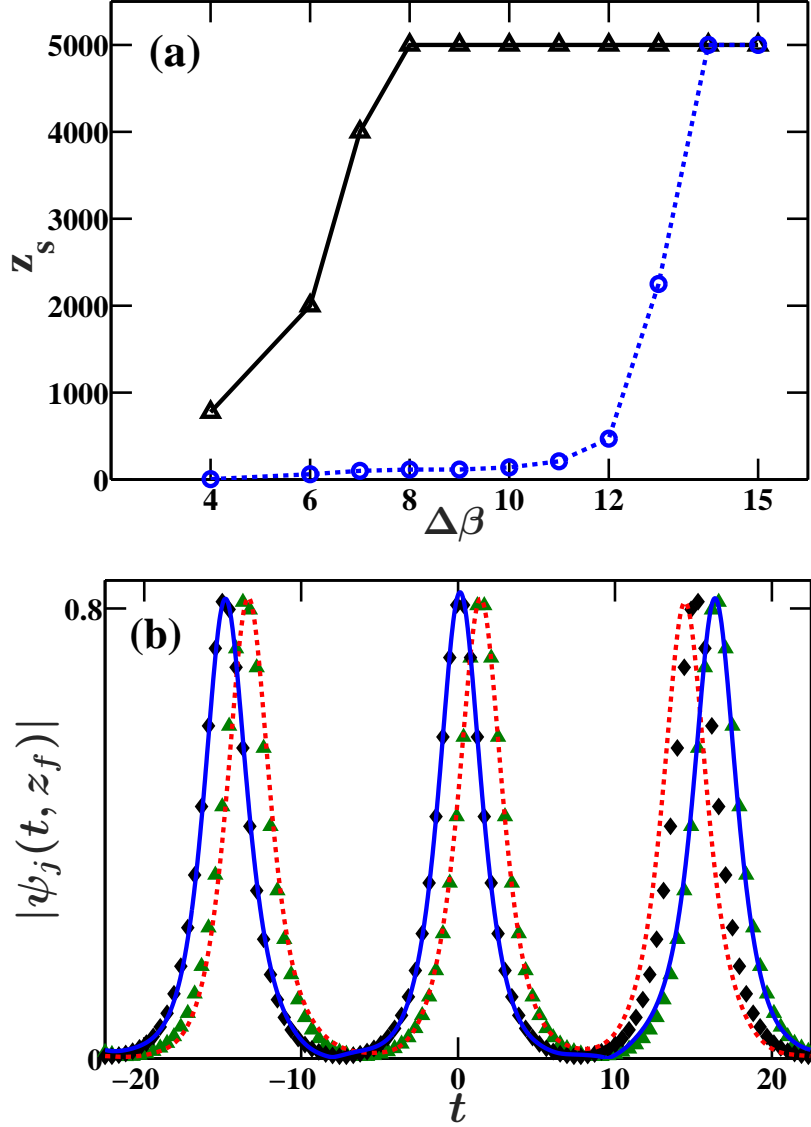


FIG. 5: (a) Stable propagation distance z_s vs frequency spacing $\Delta\beta$ for two-channel waveguide coupler transmission with frequency dependent linear loss and $\gamma = 2$, $T = 15$, $g_L = 0.5$, $g_{eq} = 0$, $\rho = 10$, and $W = \Delta\beta/2$. The solid black line is the result obtained by numerical solution of Eqs. (1) and (2). The dashed blue line is the result obtained by the simulations for two-channel transmission in a single lossless waveguide with $\gamma = 2$ and $T = 15$. (b) The final pulse patterns $|\psi_j(t, z_f)|$, where $z_f = 5000$, in two-channel waveguide coupler transmission with $\Delta\beta = 12$. The symbols are the same as in Fig. 2(b).

the abrupt decrease of $\eta_j(z)$ in the interval $150 \leq z \leq 175$, we analyze the z dependence of radiative sideband amplitudes, defined as $|\hat{\psi}_1(\beta_2(0), z)|$ and $|\hat{\psi}_2(\beta_1(0), z)|$ for $j = 1$ and $j = 2$, respectively. As seen in Figures 6(c) and 7, sideband amplitudes exhibit different behavior for $0 \leq z < 120$, $120 \leq z < 200$, and $200 \leq z \leq 5000$, which correspond to the three intervals observed for soliton amplitude dynamics. More specifically, for $0 \leq z < 120$, sideband amplitudes are smaller than 10^{-3} and are slowly increasing, for $120 \leq z < 200$, sideband amplitudes increase up to a maximum of 0.321 at $z = 160$ and then decrease to below 10^{-4} at $z = 200$, while for $200 \leq z \leq 5000$, sideband amplitudes remain smaller than 2×10^{-4} . Thus, the steep drop of $\eta_j(z)$ for $150 \leq z \leq 175$ is related to the growth and subsequent decay of the radiative sidebands in the interval $120 \leq z < 200$. This can be explained by noting that as the radiative sidebands grow, energy is rapidly transferred from a localized soliton form to a nonlocalized form, which is accompanied by the steep decay of soliton amplitudes. Additionally, the fast decay of the sidebands is a result of the strong linear loss g_L at frequencies $\beta_2(0)$ for $j = 1$ and $\beta_1(0)$ for $j = 2$. Note that the sharp drop in $\eta_j(z)$ and the associated growth and disappearance of the radiative sidebands can be described as a dynamic phase transition, which is similar to the transition of one phase of matter to another. Indeed, one can consider the solitons and the radiation to be two different “phases”. The abrupt disappearance of the radiation due to the presence of linear loss can then be viewed as a transition from an unstable transmission state, in which both phases exist in the waveguide, to a stable state, in which only the soliton “phase” exists.

The waveguide couplers with net linear loss have a major disadvantage due to the decay of soliton amplitudes. This problem can be overcome in waveguide couplers with linear gain-loss by introducing the net linear gain g_{eq} at a frequency interval of width W centered about $\beta_j(0)$. We investigate two-channel soliton transmission in waveguide couplers with linear gain-loss by performing simulations with Eqs. (1) and (2) with $N = 2$ and $g_{eq} > 0$. To enable comparison with the results of Figures 5 and 6, we discuss the results of simulations with the same parameter values, i.e., $\gamma = 2$, $T = 15$, $g_L = 0.5$, $\rho = 10$, and $W = \Delta\beta/2$. We find that soliton amplitudes exhibit different dynamic behavior in the frequency spacing intervals $4 \leq \Delta\beta < 8$, $8 \leq \Delta\beta < 14$, and $\Delta\beta \geq 14$, which are the same intervals observed for waveguide couplers with net linear loss. For $4 \leq \Delta\beta < 8$, amplitude values are approximately constant until transmission destabilization, while for $\Delta\beta \geq 14$, the amplitudes are approximately constant throughout the propagation. In contrast, for

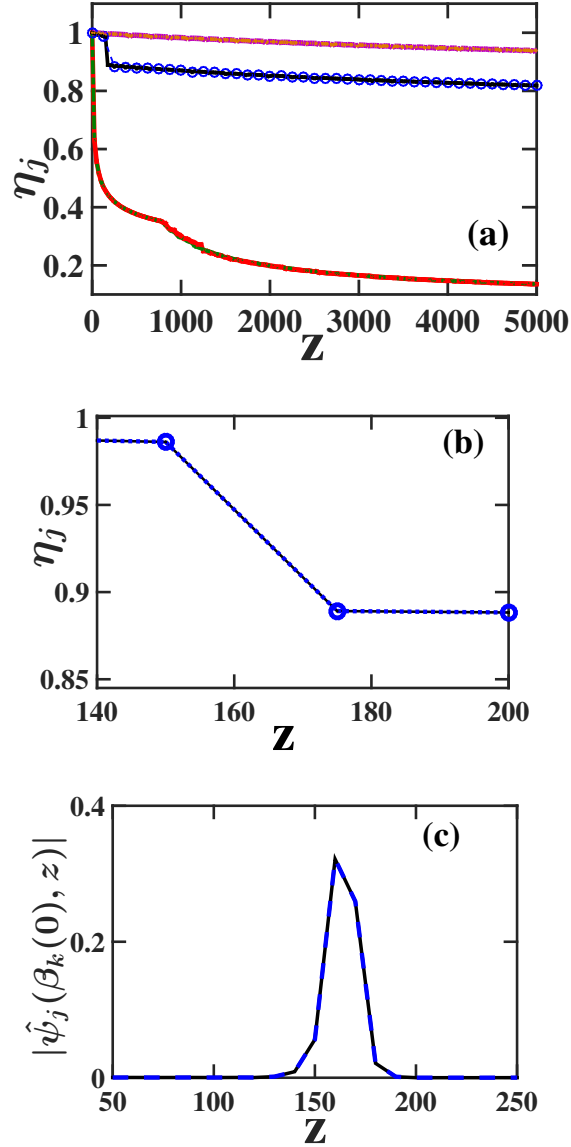


FIG. 6: (a) The z dependence of soliton amplitudes η_j for two-channel waveguide coupler transmission with frequency dependent linear loss and $\gamma = 2$, $T = 15$, $g_L = 0.5$, $g_{eq} = 0$, $\rho = 10$, and $W = \Delta\beta/2$. The solid red, solid black, and dashed-dotted purple curves correspond to $\eta_1(z)$ obtained by numerical simulations with Eqs. (1) and (2) for $\Delta\beta = 4$, $\Delta\beta = 12$, and $\Delta\beta = 14$. The dashed-dotted-dotted green, circle-dashed blue, and short dashed-dotted orange curves represent $\eta_2(z)$ obtained by the simulations for $\Delta\beta = 4$, $\Delta\beta = 12$, and $\Delta\beta = 14$. (b) Magnified versions of the $\eta_j(z)$ curves for $\Delta\beta = 12$ in the interval $140 \leq z \leq 200$. (c) The z dependence of radiative sideband amplitudes $|\hat{\psi}_1(\beta_2(0), z)|$ (solid black line) and $|\hat{\psi}_2(\beta_1(0), z)|$ (dashed blue line), obtained by the simulations for $\Delta\beta = 12$.

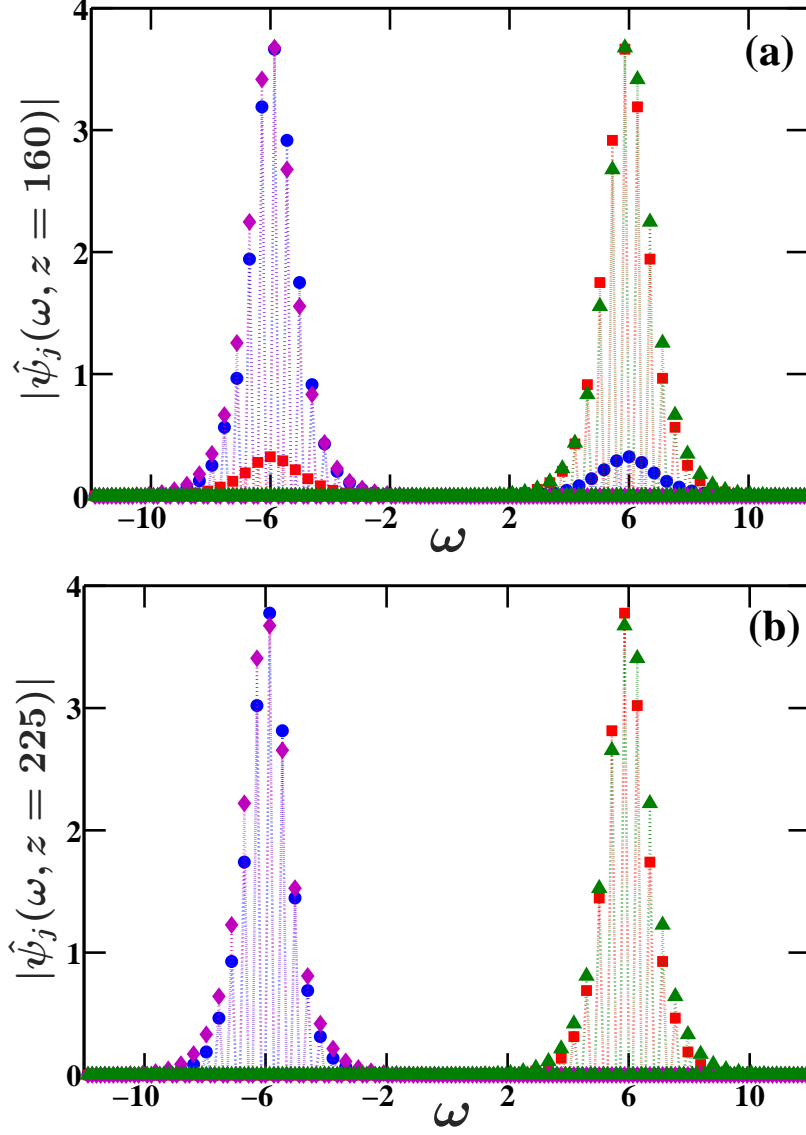


FIG. 7: The Fourier transforms of the soliton patterns $|\hat{\psi}_j(\omega, z)|$ in two-channel waveguide coupler transmission with frequency dependent linear loss for $\Delta\beta = 12$ and the same values of γ , T , g_L , g_{eq} , ρ , and W as in Fig. 6. (a) $|\hat{\psi}_j(\omega, z)|$ at $z = 160$. (b) $|\hat{\psi}_j(\omega, z)|$ at $z = 225$. The symbols are the same as in Fig. 2(a)

$8 \leq \Delta\beta < 14$, the amplitudes exhibit stable oscillations throughout the propagation. Figure 8(a) shows the oscillatory dynamics for $\Delta\beta = 10$ and $g_{eq} = 3.9 \times 10^{-4}$. As can be seen, the amplitudes undergo a step decrease, followed by oscillations about the value $\eta_s = 0.86$. Additionally, as seen in Fig. 8(b), pulse distortion at $z_f = 5000$ is small, although the solitons within each sequence experience position shifts relative to one another. To check if

the oscillations of soliton amplitudes are caused by radiative sideband dynamics, we analyze the z dependence of radiative sideband amplitudes $|\hat{\psi}_1(\beta_2(0), z)|$ and $|\hat{\psi}_2(\beta_1(0), z)|$. As seen in Fig. 8(c), the amplitudes of the radiative sidebands experience alternating “periods” of growth and decay. Furthermore, the points where the sidebands are maximal are located near the beginnings of the relatively short intervals, where soliton amplitudes are decreasing [see Fig. 8(a)]. Based on these observations, we conclude that the oscillatory dynamics of soliton amplitudes is caused by decay and regeneration of the radiative sidebands. This can be explained by noting that as the sidebands grow, energy is transferred from a localized soliton form to a nonlocalized form. The strong linear loss g_L outside the central frequency intervals leads to relatively fast decay of the radiative sidebands, which is accompanied by a decrease in soliton amplitudes. Furthermore, the weak linear gain g_{eq} at the central frequency intervals leads to slow growth of soliton amplitudes at the subsequent waveguide spans and to the observed oscillatory dynamics.

C. Three-channel transmission

It is important to investigate whether the results obtained in subsection IIIB for transmission stabilization in a two-channel system remain valid as more frequency channels are added. For this purpose, we turn to discuss the results of numerical simulations for three-channel transmission, starting with transmission in a single lossless waveguide. As seen in Fig. 9, transmission destabilization is caused by resonant formation of radiative sidebands in a manner similar to the two-channel case. Moreover, the largest radiative sidebands of the j th sequence appear at frequencies $\beta_k(0)$ of the neighboring soliton sequences. That is, the largest sideband of the $j = 1$ sequence is formed at frequency $\beta_2(0)$, the $j = 2$ sidebands are formed at frequencies $\beta_1(0)$ and $\beta_3(0)$, and the $j = 3$ sideband is formed at frequency $\beta_2(0)$. Similar to the two-channel case, the formation of the radiative sidebands leads to pulse distortion, which first appears as fast oscillations in the soliton patterns. The growth of the radiative sidebands with increasing propagation distance eventually leads to the destruction of the soliton patterns. Furthermore, the distances z_u , at which instability first appears in three-channel transmission, are significantly shorter compared with the distances z_u observed for two-channel transmission. For example, for parameter values $\gamma = 2$, $T = 15$, and $\Delta\beta = 12$, used in Figs. 2 and 9, $z_u = 74$ for $N = 3$ compared with $z_u = 470$ for $N = 2$.

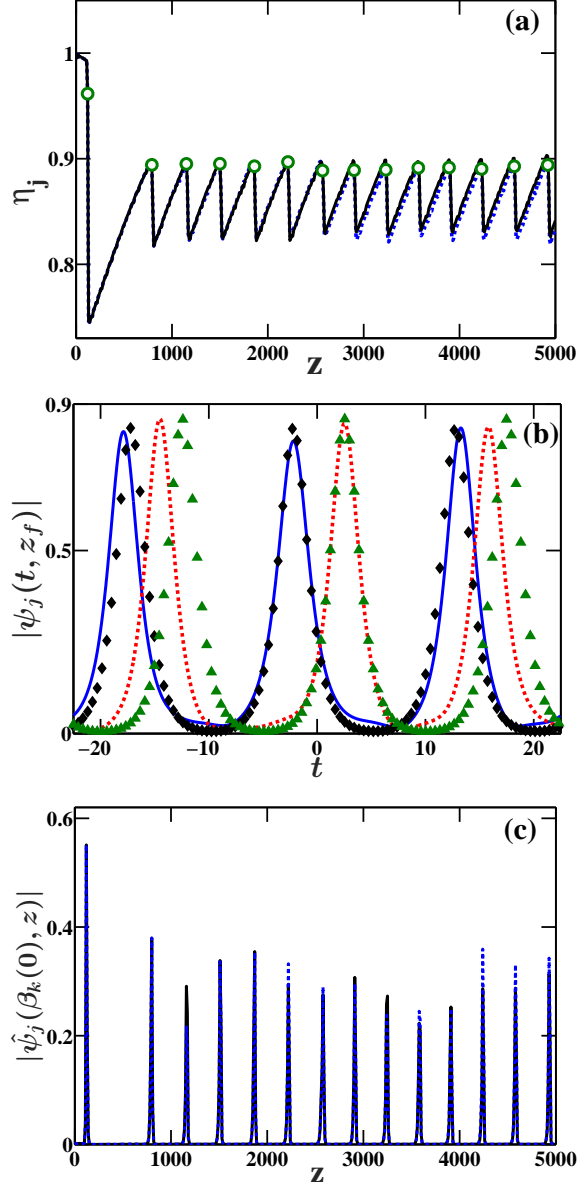


FIG. 8: (a) The z dependence of soliton amplitudes η_j for two-channel waveguide coupler transmission with frequency dependent linear gain-loss and $\gamma = 2$, $T = 15$, $\Delta\beta = 10$, $g_L = 0.5$, $g_{eq} = 3.9 \times 10^{-4}$, $\rho = 10$, and $W = 5$. The solid black and dashed blue lines correspond to $\eta_j(z)$ with $j = 1, 2$, as obtained by numerical solution of Eqs. (1) and (2). The green circles indicate the distances at which radiative sideband amplitudes attain their maxima. (b) The final pulse patterns $|\psi_j(t, z_f)|$, where $z_f = 5000$. The symbols are the same as in Fig. 2(b). (c) The z dependence of radiative sideband amplitudes $|\hat{\psi}_1(\beta_2(0), z)|$ (solid black line) and $|\hat{\psi}_2(\beta_1(0), z)|$ (dashed blue line), obtained by the simulations.

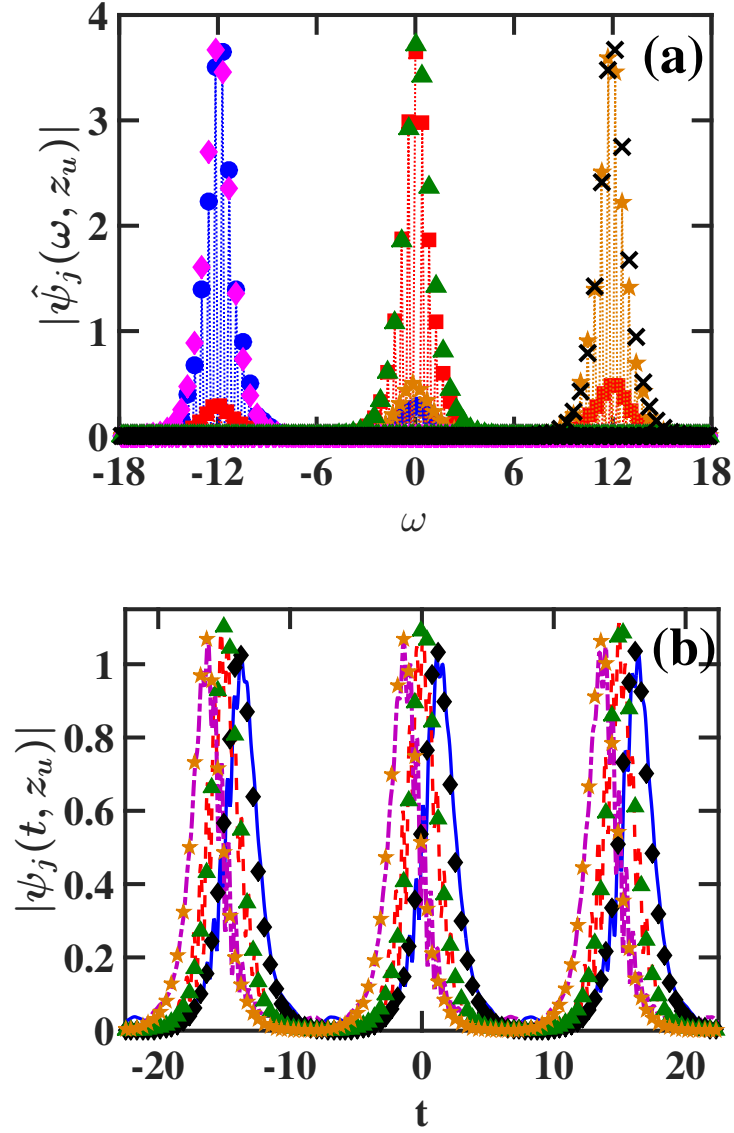


FIG. 9: (a) The Fourier transforms of the soliton patterns at the onset of instability $|\hat{\psi}_j(\omega, z_u)|$, where $z_u = 74$, for three-channel transmission in a single lossless waveguide with $\gamma = 2$, $T = 15$, and $\Delta\beta = 12$. The blue circles, red squares, and orange stars represent $|\hat{\psi}_j(\omega, z_u)|$ with $j = 1, 2$, and 3 , obtained by numerical solution of Eq. (1), while the magenta diamonds, green triangles and black crosses correspond to the theoretical prediction. (b) The soliton patterns at the onset of instability $|\psi_j(t, z_u)|$ for three-channel transmission with the same parameters used in (a). The solid blue, dashed red, and dash-dot purple lines correspond to $|\psi_j(t, z_u)|$ with $j = 1, 2$, and 3 , obtained by the simulations, while the black diamonds, green triangles and orange stars correspond to the theoretical prediction.

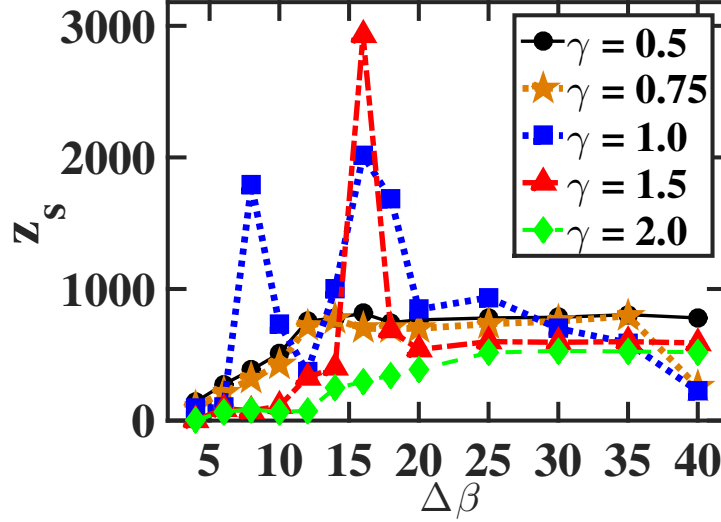


FIG. 10: Stable propagation distance z_s vs frequency spacing $\Delta\beta$ for three-channel transmission in a single lossless waveguide with $T = 15$. The black circles, orange stars, blue squares, red triangles, and green diamonds represent the results obtained by the simulations for $\gamma = 0.5, 0.75, 1.0, 1.5$, and 2.0 , respectively.

Next, we discuss the dependence of transmission stability for three-channel transmission in a single lossless waveguide on the frequency spacing $\Delta\beta$ and the Kerr nonlinearity coefficient γ . Figure 10 shows the stable propagation distances z_s as functions of the frequency spacing $\Delta\beta$ for $T = 15$ and $\gamma = 0.5, 0.75, 1.0, 1.5, 2.0$. It is observed that the largest z_s values are obtained with $\gamma = 0.5$ for $4 \leq \Delta\beta \leq 6$, $11 \leq \Delta\beta < 13$, and $25 < \Delta\beta \leq 40$; with $\gamma = 1.0$ for $6 < \Delta\beta < 11$, $13 \leq \Delta\beta < 15$, and $17 \leq \Delta\beta \leq 25$; and with $\gamma = 1.5$ for $15 \leq \Delta\beta < 17$. Thus, there is no single value of γ , which is optimal over the entire frequency spacing interval $4 \leq \Delta\beta \leq 40$. This behavior is sharply different from the one observed for two-channel transmission, where the value $\gamma = 1.0$ is found to be optimal over the entire interval $4 \leq \Delta\beta \leq 40$. Furthermore, the z_s values obtained for $N = 3$ are significantly smaller than the ones obtained for $N = 2$. For example, for $20 \leq \Delta\beta \leq 40$ the z_s values for three-channel transmission are smaller than 1000 for all γ values, while the corresponding z_s values for two-channel transmission are equal to 5000 for $\gamma = 1.0, 1.5$, and 2.0 .

We now turn to analyze three-channel transmission in a waveguide coupler with frequency dependent linear loss. Our goal is to check whether the introduction of frequency dependent linear loss in a waveguide coupler leads to enhancement of transmission stability in three-

channel systems. For this purpose, we numerically solve Eqs. (1) and (2) with $N = 3$, $g_{eq} = 0$, and $g_L = 0.5$ for $4 \leq \Delta\beta \leq 40$. To enable comparison with the results obtained for two-channel transmission, we present here the results of simulations with the same physical parameter values as the ones used in Figs. 5 and 6. That is, we use $\gamma = 2$, $T = 15$, $\rho = 10$, and $W = \Delta\beta/2$. Figure 11(a) shows the stable propagation distance z_s vs frequency spacing $\Delta\beta$ as obtained in the simulations together with the values obtained for transmission in a single lossless waveguide. We observe that $z_s = z_f = 5000$ for all $\Delta\beta$ values in the interval $4 \leq \Delta\beta \leq 40$. Additionally, as seen in Fig. 11(b), pulse-pattern distortion is relatively small at the final propagation distance. Based on these observations we conclude that three-channel transmission through the waveguide coupler is stable throughout the propagation for any $\Delta\beta$ value in the interval $4 \leq \Delta\beta \leq 40$. Surprisingly, the z_s values obtained for three-channel waveguide coupler transmission for $4 \leq \Delta\beta \leq 7$ are larger than the corresponding values obtained for two-channel waveguide coupler transmission by factors ranging between 6.45 for $\Delta\beta = 4$ and 1.25 for $\Delta\beta = 7$. Furthermore, the z_s values obtained for three-channel waveguide coupler transmission are larger than the values obtained for three-channel single waveguide transmission by factors ranging between 1250 for $\Delta\beta = 4$ and 9.43 for $\Delta\beta = 30$. Note that these enhancement factors are significantly larger than the enhancement factors for two-channel transmission, which are smaller than 172.3 for all $\Delta\beta$ values in the interval $4 \leq \Delta\beta \leq 40$.

Further insight into the mechanisms leading to transmission stabilization in waveguide couplers with frequency dependent linear loss is gained by analyzing the z dependence of soliton amplitudes. Similar to the two-channel case, we find three qualitatively different dependences of soliton amplitudes on z in the frequency spacing intervals $4 \leq \Delta\beta < 8$, $8 \leq \Delta\beta < 14$, and $\Delta\beta \geq 14$. Figure 12(a) shows the $\eta_j(z)$ curves obtained by the simulations for three representative $\Delta\beta$ values, $\Delta\beta = 4$, $\Delta\beta = 12$, and $\Delta\beta = 14$. We observe that for $\Delta\beta = 4$ and $\Delta\beta = 14$, the soliton amplitudes gradually decrease to their final values. For $\Delta\beta = 12$, the amplitudes of the solitons in the first frequency channel also decrease gradually throughout the propagation. However, the amplitudes of the solitons in the second and third frequency channels exhibit a more complicated dependence on z , which is very similar to the one observed for two-channel waveguide coupler transmission with $\Delta\beta = 12$. More specifically, soliton amplitudes in the second and third channels gradually decrease for $0 \leq z < 150$, but then undergo a steep decrease in the interval $150 \leq z \leq 200$, followed by

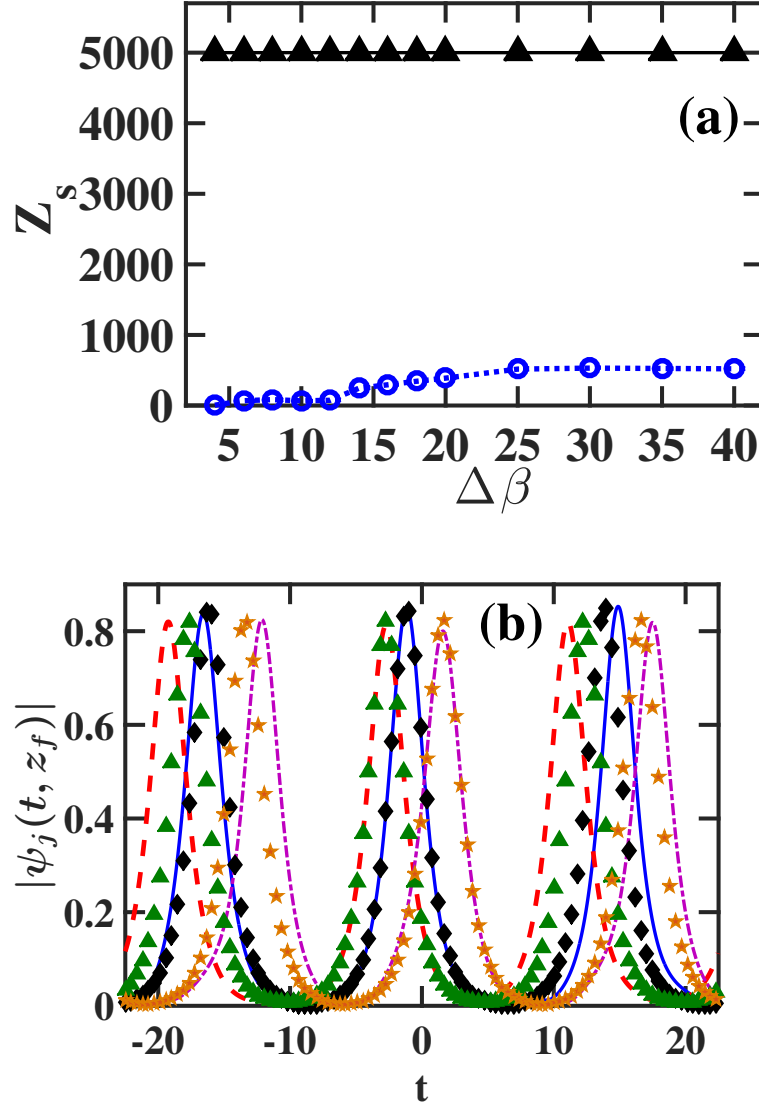


FIG. 11: (a) Stable propagation distance z_s vs frequency spacing $\Delta\beta$ for three-channel waveguide coupler transmission with frequency dependent linear loss and $\gamma = 2$, $T = 15$, $g_L = 0.5$, $g_{eq} = 0$, $\rho = 10$, and $W = \Delta\beta/2$. The solid black line is the result obtained by numerical solution of Eqs. (1) and (2). The dashed blue line is the result obtained by the simulations for three-channel transmission in a single lossless waveguide with $\gamma = 2$ and $T = 15$. (b) The final pulse patterns $|\psi_j(t, z_f)|$, where $z_f = 5000$, in three-channel waveguide coupler transmission with $\Delta\beta = 12$. The symbols are the same as in Fig. 9(b).

another gradual decrease for $200 < z \leq 5000$ [see Figures 12(a) and 12(b)].

The behavior of $\eta_j(z)$ in the interval $150 \leq z \leq 200$ can be explained by analyzing the z dependence of radiative sideband amplitudes $|\hat{\psi}_j(\beta_k(0), z)|$, where $1 \leq j \leq 3$, $1 \leq k \leq 3$, and $j \neq k$. Figure 12(c) shows the z dependence of the radiative sideband amplitudes in the interval $125 \leq z \leq 250$, while Fig. 13 shows the Fourier transforms of the soliton patterns at $z = 175$ and $z = 250$. As can be seen from these figures, the sideband amplitudes $|\hat{\psi}_2(\beta_3(0), z)|$ and $|\hat{\psi}_3(\beta_2(0), z)|$ attain a sharp maximum at $z = 177.5$ with maximal values of 0.456 and 0.465, respectively. The increase of these sideband amplitudes is followed by a drop to values smaller than 10^{-3} at $z = 205$. The formation and subsequent decay of the main radiative sidebands for the $j = 2$ and $j = 3$ channels in the interval $150 \leq z \leq 200$ explains the sharp drop in $\eta_2(z)$ and $\eta_3(z)$ observed in this interval. Indeed, the formation of the sidebands leads to energy transfer from a localized soliton form to a nonlocalized radiative form, which results in the steep drop of $\eta_2(z)$ and $\eta_3(z)$. Additionally, the strong linear loss g_L at frequencies $\beta_3(0)$ for $j = 2$ and $\beta_2(0)$ for $j = 3$ leads to the relatively fast decay of the sidebands following their formation. We note that the evolution of $\eta_2(z)$ and $\eta_3(z)$ in the three-channel waveguide coupler is in fact quite similar to the evolution of $\eta_1(z)$ and $\eta_2(z)$ in the two-channel waveguide coupler.

Figure 12(c) also shows that the sideband amplitudes $|\hat{\psi}_1(\beta_2(0), z)|$ and $|\hat{\psi}_2(\beta_1(0), z)|$ attain a maximum at $z = 185$ with maximal values of 0.117 and 0.111, respectively. The increase of these sideband amplitudes is followed by a decrease to below 10^{-3} values at $z = 257.5$. Thus, the formation and subsequent decay of the $j = 1$ sideband at frequency $\beta_2(0)$ in an interval centered about $z = 185$ explains the observed drop in the value of $\eta_1(z)$ in this interval. Additionally, the sideband amplitudes $|\hat{\psi}_1(\beta_3(0), z)|$ and $|\hat{\psi}_3(\beta_1(0), z)|$ attain a maximum at $z = 177.5$, but the corresponding maximal values are smaller than 10^{-3} , and as a result, do not significantly affect the amplitude dynamics. The relatively small values of $|\hat{\psi}_1(\beta_3(0), z)|$ and $|\hat{\psi}_3(\beta_1(0), z)|$ compared with the other four sideband amplitudes indicate that the magnitude of radiative sidebands decreases as the absolute value of the frequency difference $|\beta_j(0) - \beta_k(0)|$ increases.

We conclude the discussion of three-channel transmission by considering propagation in waveguide couplers with frequency dependent linear gain and loss. As explained in section II, in these waveguide couplers, the weak linear gain g_{eq} in the frequency interval $(\beta_j(0) - W/2, \beta_j(0) + W/2]$ is expected to enable soliton propagation without amplitude decay. To

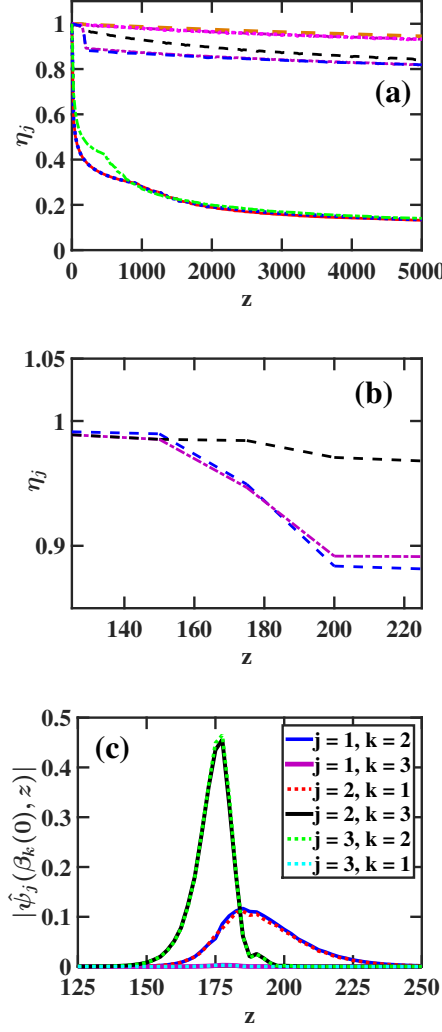


FIG. 12: (a) The z dependence of soliton amplitudes η_j for three-channel waveguide coupler transmission with frequency dependent linear loss and $\gamma = 2$, $T = 15$, $g_L = 0.5$, $g_{eq} = 0$, $\rho = 10$, and $W = \Delta\beta/2$. The solid red, dashed black, and solid purple curves correspond to $\eta_1(z)$ obtained by numerical simulations with Eqs. (1) and (2) for $\Delta\beta = 4$, $\Delta\beta = 12$, and $\Delta\beta = 14$. The dashed-dotted-dotted green, short dashed blue, and short dashed-dotted orange curves represent $\eta_2(z)$ obtained by the simulations for $\Delta\beta = 4$, $\Delta\beta = 12$, and $\Delta\beta = 14$. The dotted blue, dashed-dotted purple, and dotted green curves represent $\eta_3(z)$ obtained by the simulations for $\Delta\beta = 4$, $\Delta\beta = 12$, and $\Delta\beta = 14$. (b) Magnified versions of the $\eta_j(z)$ curves for $\Delta\beta = 12$ in the interval $125 \leq z \leq 250$. (c) The z dependence of radiative sideband amplitudes $|\hat{\psi}_1(\beta_2(0), z)|$ (solid blue line), $|\hat{\psi}_1(\beta_3(0), z)|$ (solid purple line), $|\hat{\psi}_2(\beta_1(0), z)|$ (dashed red line), $|\hat{\psi}_2(\beta_3(0), z)|$ (solid black line), $|\hat{\psi}_3(\beta_1(0), z)|$ (dashed light blue line), and $|\hat{\psi}_3(\beta_2(0), z)|$ (dashed green line) obtained by the simulations for $\Delta\beta = 12$.

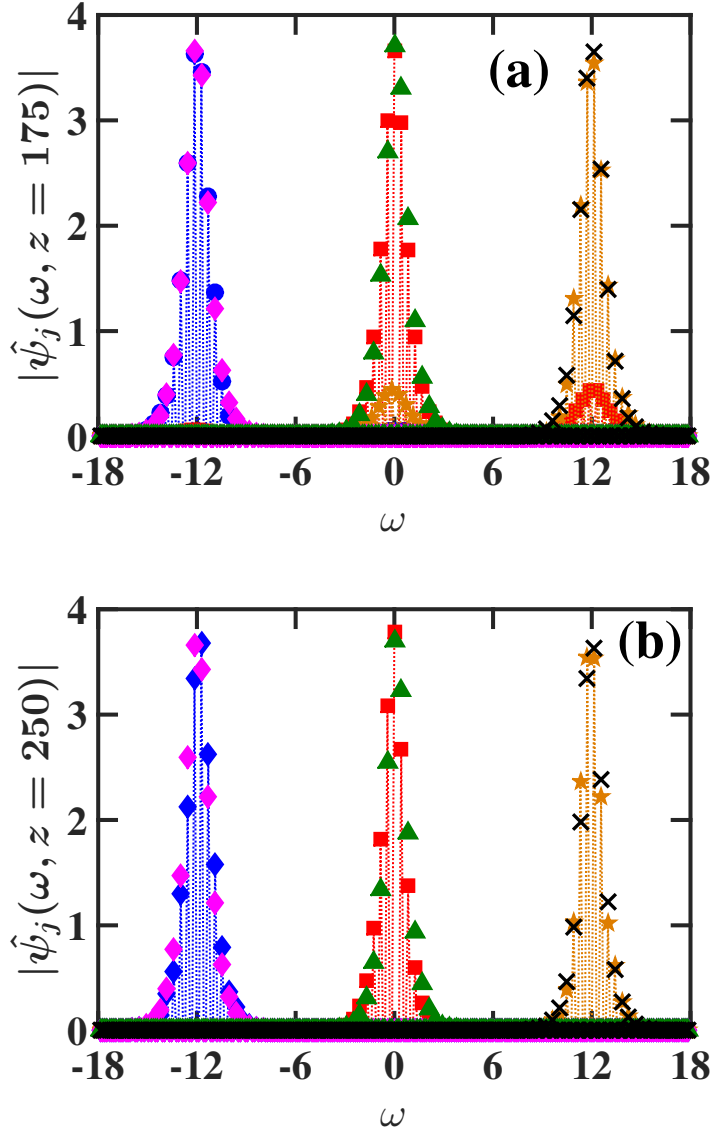


FIG. 13: The Fourier transforms of the soliton patterns $|\hat{\psi}_j(\omega, z)|$ in three-channel waveguide coupler transmission with frequency dependent linear loss for $\Delta\beta = 12$ and the same values of γ , T , g_L , g_{eq} , ρ , and W as in Fig. 12. (a) $|\hat{\psi}_j(\omega, z)|$ at $z = 175$. (b) $|\hat{\psi}_j(\omega, z)|$ at $z = 250$. The symbols are the same as in Fig. 9(a)

check if such stable propagation can indeed be realized, we numerically solve Eqs. (1) and (2) with $N = 3$ and with a value of g_{eq} , which is determined by Eq. (5). To enable comparison with the results presented in Fig. 8 for two-channel transmission, we discuss the results of numerical simulations with the same set of physical parameter values. That

is, we use $\gamma = 2$, $T = 15$, $\Delta\beta = 10$, $g_{eq} = 3.9 \times 10^{-4}$, $g_L = 0.5$, $\rho = 10$, and $W = 5$. Figure 14(a) shows the z dependence of soliton amplitudes obtained by the simulations. It is seen that the amplitudes undergo a sharp drop, which is followed by oscillations about values of $\eta_{s1} = 0.940$, $\eta_{s2} = 0.768$, and $\eta_{s3} = 0.947$, for $j = 1$, $j = 2$ and $j = 3$, respectively. In addition, as seen in Fig. 14(b), the soliton shape is retained at $z_f = 5000$, although the pulses in each sequence experience significant position shifts relative to one another. We note that η_{s2} is significantly smaller than η_{s1} and η_{s3} . In addition, the overall oscillatory dynamics of soliton amplitudes is similar to the one observed in two-channel transmission, although the pattern of oscillations is more complex for $N = 3$ compared with $N = 2$.

Similar to the situation in two-channel transmission, the oscillations of soliton amplitudes can be related to radiative sideband dynamics. We study this dynamics by analyzing the z -dependence of sideband amplitudes $|\hat{\psi}_j(\beta_k(0), z)|$, where $1 \leq j \leq 3$, $1 \leq k \leq 3$, and $j \neq k$. Figure 15(a) shows the z dependence of sideband amplitudes $|\hat{\psi}_1(\beta_2(0), z)|$ and $|\hat{\psi}_2(\beta_1(0), z)|$, Fig. 15(b) shows the z dependence of $|\hat{\psi}_2(\beta_3(0), z)|$ and $|\hat{\psi}_3(\beta_2(0), z)|$, while Fig. 15(c) shows the z dependence of $|\hat{\psi}_1(\beta_3(0), z)|$ and $|\hat{\psi}_3(\beta_1(0), z)|$. All curves in Fig. 15 are obtained by numerical solution of Eqs. (1) and (2). We note that the values of $|\hat{\psi}_1(\beta_3(0), z)|$ and $|\hat{\psi}_3(\beta_1(0), z)|$ are smaller than 0.041 throughout the propagation, and therefore these sidebands do not significantly affect amplitude dynamics. We therefore focus attention on dynamics of the four strongest sidebands $|\hat{\psi}_1(\beta_2(0), z)|$, $|\hat{\psi}_2(\beta_1(0), z)|$, $|\hat{\psi}_2(\beta_3(0), z)|$, and $|\hat{\psi}_3(\beta_2(0), z)|$. As seen in Figure 15, the radiative sideband amplitudes experience alternating “periods” of growth and decay, similar to the situation in two-channel transmission. Furthermore, the distances at which sideband amplitudes attain their maxima for the four strongest sidebands are located inside the relatively short intervals, where soliton amplitudes are decreasing. Therefore, the dynamics of the radiative sidebands can indeed be related to the oscillatory dynamics of soliton amplitudes. More specifically, as the sidebands grow, energy is transferred from a localized soliton form to a nonlocalized form, resulting in a decrease in soliton amplitudes. The strong linear loss g_L outside the central frequency intervals leads to a relatively fast decay of the sidebands, and as a result, the sidebands maxima are very narrow with respect to z . Additionally, the weak linear gain g_{eq} at the central frequency intervals leads to the slow growth of soliton amplitude at the subsequent waveguide spans and to the overall oscillatory dynamics.

Figure 15 also provides an explanation for the smaller value of η_{s2} compared to η_{s1} and

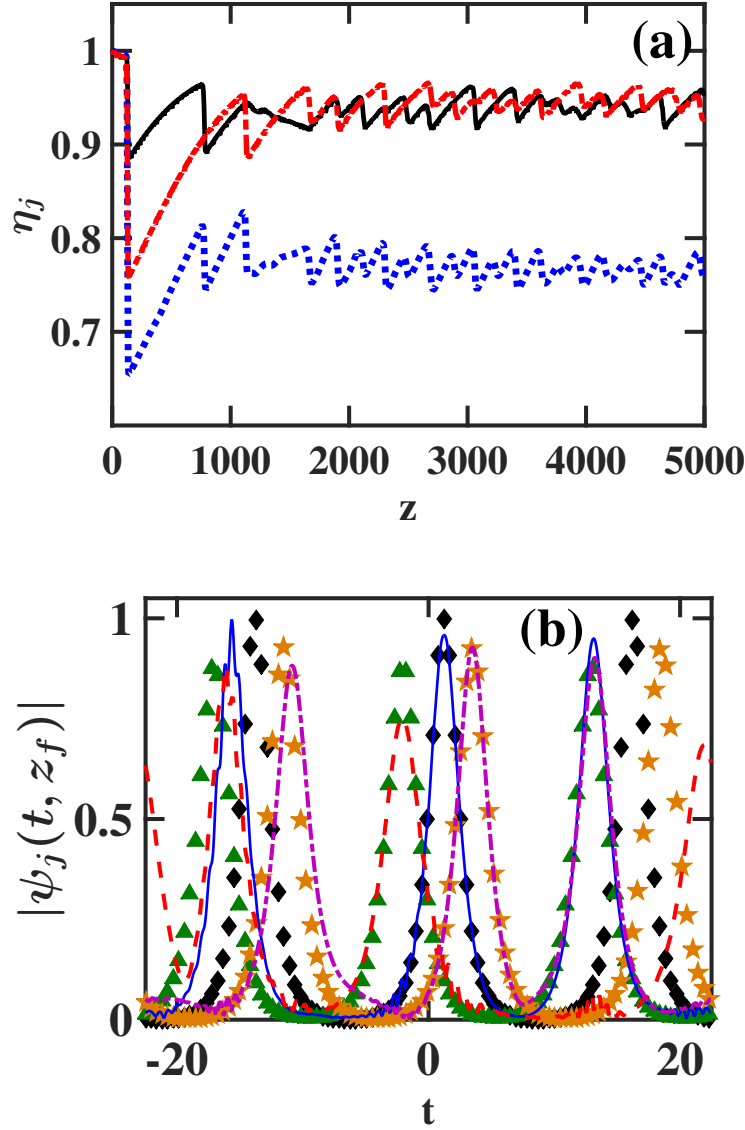


FIG. 14: (a) The z dependence of soliton amplitudes η_j for three-channel waveguide coupler transmission with frequency dependent linear gain-loss and $\gamma = 2$, $T = 15$, $\Delta\beta = 10$, $g_L = 0.5$, $g_{eq} = 3.9 \times 10^{-4}$, $\rho = 10$, and $W = 5$. The solid black, dashed blue, and dashed-dotted red lines correspond to $\eta_j(z)$ with $j = 1, 2, 3$, as obtained by numerical solution of Eqs. (1) and (2). (b) The final pulse patterns $|\psi_j(t, z_f)|$, where $z_f = 5000$. The symbols are the same as in Fig. 9(b).

η_{s3} . Indeed, during the first (and largest) drop in soliton amplitudes, the solitons in the $j = 2$ sequence lose energy due to formation of radiative sidebands at *both* $\beta_1(0)$ and $\beta_3(0)$. In contrast, the $j = 1$ and $j = 3$ solitons lose energy almost entirely due to formation of radiative sidebands at $\beta_2(0)$, since the sidebands at $\beta_3(0)$ for $j = 1$ and at $\beta_1(0)$ for

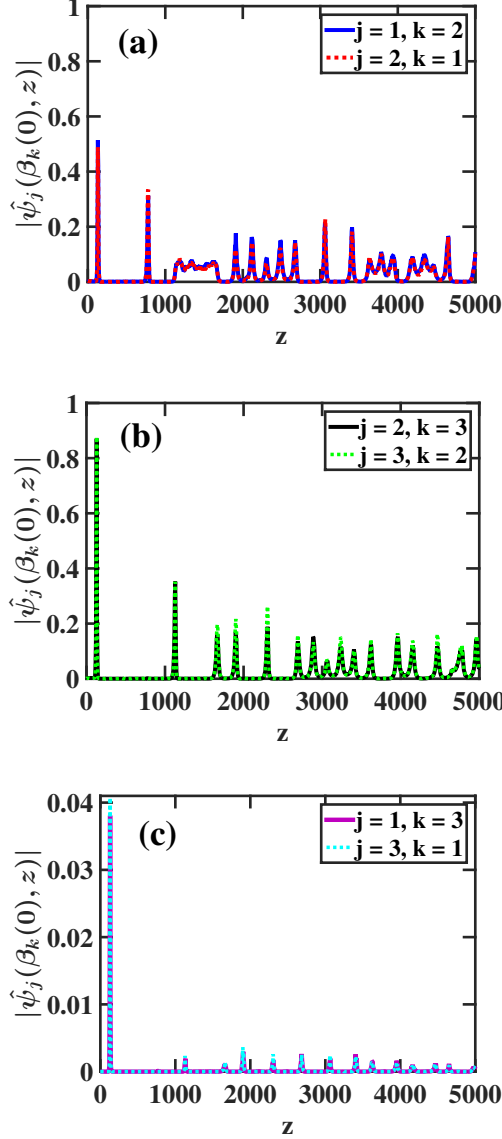


FIG. 15: The z dependence of radiative sideband amplitudes for three-channel waveguide coupler transmission with the same physical parameter values as in Fig. 14. (a) $|\hat{\psi}_1(\beta_2(0), z)|$ and $|\hat{\psi}_2(\beta_1(0), z)|$ vs z . (b) $|\hat{\psi}_2(\beta_3(0), z)|$ and $|\hat{\psi}_3(\beta_2(0), z)|$ vs z . (c) $|\hat{\psi}_1(\beta_3(0), z)|$ and $|\hat{\psi}_3(\beta_1(0), z)|$ vs z . All curves represent results obtained by simulations with Eqs. (1) and (2). The symbols are the same as in Fig. 12(c).

$j = 3$ are very small. In addition, the complicated pattern of radiative sideband growth and decay shown in Fig. 15 is responsible for the more complex pattern of amplitude oscillations observed in three-channel transmission compared with two-channel transmission [compare Fig. 14(a) with Fig. 8(a) and Fig. 15 with Fig. 8(c)].

IV. CONCLUSIONS

In summary, we made several major theoretical steps towards realizing stable long-distance multichannel soliton transmission in Kerr nonlinear waveguide loops. We found that transmission destabilization in a single lossless waveguide is caused by resonant formation of radiative sidebands due to intersequence cross-phase modulation. We then showed that in two-channel systems, significant enhancement of the stable propagation distance, which holds over a wide range of interchannel frequency spacing values, is obtained by optimization with respect to the Kerr nonlinearity coefficient γ . In contrast, we found that in three-channel transmission in a single lossless waveguide, no single value of the Kerr nonlinearity coefficient is optimal for the entire interval of interchannel frequency spacings that we examined. Moreover, we developed a general method for transmission stabilization, based on frequency dependent linear gain-loss in Kerr nonlinear waveguide couplers, and implemented the method in two-channel and three-channel transmission. We showed that the introduction of frequency dependent loss leads to significant enhancement of transmission stability even for non-optimal γ values via decay of radiative sidebands, which can be described as a dynamic phase transition. For waveguide couplers with frequency dependent linear gain-loss, we observed stable oscillations of soliton amplitudes due to decay and regeneration of radiative sidebands. Transmission stabilization was achieved without dispersion-management or filtering.

Acknowledgments

Q.M.N. is supported by the Vietnam National Foundation for Science and Technology Development (NAFOSTED). D.C. is grateful to the Mathematics Department of NJCU for providing technological support for the computations.

-
- [1] G.P. Agrawal, Nonlinear Fiber Optics, Academic, San Diego, CA, 2001.
 - [2] L.F. Mollenauer and J.P. Gordon, Solitons in Optical Fibers: Fundamentals and Applications, Academic, San Diego, CA, 2006.

- [3] E. Iannone, F. Matera, A. Mecozzi, and M. Settembre, *Nonlinear Optical Communication Networks*, Wiley, New York, 1998.
- [4] Q. Lin, O.J. Painter, and G.P. Agrawal, *Opt. Express* 15, (2007) 16604.
- [5] M.A. Foster, A.C. Turner, M. Lipson, and A.L. Gaeta, *Opt. Express* 16, (2008) 1300.
- [6] H. Zhang, D.Y. Tang, X. Wu, and L.M. Zhao, *Opt. Express* 17, (2009) 12692.
- [7] X.M. Liu, D.D. Han, Z.P. Sun, C. Zeng, H. Lu, D. Mao, Y.D. Cui, and F.Q. Wang, *Sci. Rep.* 3, (2013) 2718.
- [8] Q.M. Nguyen and A. Peleg, *Opt. Commun.* 283, (2010) 3500.
- [9] A. Peleg, Q.M. Nguyen, and Y. Chung, *Phys. Rev. A* 82, (2010) 053830.
- [10] A. Peleg, Q.M. Nguyen, and T.P. Tran, arXiv:1501.06300.
- [11] A. Peleg and Y. Chung, *Phys. Rev. A* 85, (2012) 063828.
- [12] D. Chakraborty, A. Peleg, and J.-H. Jung, *Phys. Rev. A* 88, (2013) 023845.
- [13] Q.M. Nguyen, A. Peleg, and T.P. Tran, *Phys. Rev. A* 91, (2015) 013839.
- [14] The dimensionless distance z in Eq. (1) is $z = X/(2L_D)$, where X is the dimensional distance, $L_D = \tau_0^2/|\tilde{\beta}_2|$ is the dimensional dispersion length, τ_0 is the soliton width, and $\tilde{\beta}_2$ is the second-order dispersion coefficient. The dimensionless time is $t = \tau/\tau_0$, where τ is the time. $\psi_j = E_j/\sqrt{P_0}$, where E_j is proportional to the electric field of the j th sequence and P_0 is the peak power. The coefficients γ and g_{eq} are related to the dimensional Kerr nonlinearity and linear gain-loss coefficients $\tilde{\gamma}$ and \tilde{g}_{eq} by $\gamma = 2P_0\tau_0^2\tilde{\gamma}/|\tilde{\beta}_2|$ and $g_{eq} = 2\tau_0^2\tilde{g}_{eq}/|\tilde{\beta}_2|$, respectively. The solitons spectral width is $\nu_0 = 1/(\pi^2\tau_0)$ and the intersequence frequency difference is $\Delta\nu = (\pi\Delta\beta\nu_0)/2$.
- [15] For single-waveguide transmission, one should replace the N $g_j(\omega)$ functions by a single linear gain-loss function $g(\omega)$ [10].
- [16] L.F. Mollenauer and P.V. Mamyshev, *IEEE J. Quantum Electron.* 34, (1998) 2089.
- [17] L.F. Mollenauer, P.V. Mamyshev, and M.J. Neubelt, *Electron. Lett.* 32, (1996) 471.
- [18] M. Nakazawa, K. Suzuki, H. Kubota, A. Sahara, and E. Yamada, *Electron. Lett.* 33, (1997) 1233.
- [19] M. Nakazawa, K. Suzuki, E. Yoshida, E. Yamada, T. Kitoh, and M. Kawachi, *Electron. Lett.* 35, (1999) 1358.
- [20] M. Nakazawa, *IEEE J. Sel. Top. Quant. Electron.* 6, (2000) 1332.